Discovery of Globular Cluster Candidates in the Dwarf Irregular Galaxy IC 2574 Using HST/ACS Imaging

Noushin Karim[1], Michelle L. M. Collins[1], Duncan A. Forbes[2] and Justin I. Read[1]

[1]*Physics Department, University of Surrey, Guildford, GU2 7XH, UK*

[2]*Centre for Astrophysics and Supercomputing, Swinburne University, Hawthorn, VIC 3122, Australia*

28 February 2024

ABSTRACT

We report the discovery of 23 globular cluster (GC) candidates around the relatively isolated dwarf galaxy IC 2574 within the Messier 81 (M81) group, at a distance of 3.86 Mpc. We use observations from the HST Advanced Camera for Surveys (ACS) to analyse the imaging in the F814W and F555W broadband filters. Our GC candidates have luminosities ranging from $-5.9 \geq M_V \geq -10.4$ and half-light radii of $1.4 \leq r_h \leq 11.5$ pc. We find the total number of GCs (N_{GC}) = 27 ± 5 after applying completeness corrections, which implies a specific frequency of S_N = 4.0 ± 0.8, consistent with expectations based on its luminosity. The GC system appears to have a bimodal colour distribution, with 30% of the GC candidates having redder colours. We also find 5 objects with extremely blue colours that could be young star clusters linked to an intense star formation episode that occurred in IC 2574 ~1 Gyr ago. We make an independent measurement of the halo mass of IC 2574 from its kinematic data, which is rare for low mass galaxies, and find log M_{200} = 10.93 ± 0.08. We place the galaxy on the well-known GC system mass-halo mass relation and find that it agrees well with the observed near-linear relation. IC 2574 has a rich GC population for a dwarf galaxy, which includes an unusually bright ω Cen-like GC, making it an exciting nearby laboratory for probing the peculiar efficiency of forming massive GCs in dwarf galaxies.

Key words: galaxies: clusters: general – galaxies: formation – galaxies: dwarf – galaxies: individual: IC 2574

1 INTRODUCTION

Globular clusters (GCs) are among the oldest astronomical objects to exist, providing a unique probe into the early Universe and the conditions under which the first galaxies formed, making them reliable tracers of galaxy formation and evolution (Puzia et al. 2005; Strader et al. 2005; Kruijssen 2014; Orkney et al. 2019; Beasley 2020). GCs are composed of a homogeneous stellar population with similar ages, metallicities and chemical compositions, although they do show interesting spreads and correlations in their light element abundances (Osborn & Schmitt 1971; Shetrone 1996; Ivans et al. 1999; Yong et al. 2003; Gratton et al. 2004; Piotto et al. 2007; D'Antona & Caloi 2007; Carretta et al. 2009; Marino et al. 2012; Mészáros et al. 2015; Bastian & Lardo 2018; Nataf et al. 2019, and references therein). Despite complex galaxy evolution through mergers and interactions, high density GC cores can remain largely intact and retain unique characteristics of the environment in which they were born (Peñarrubia et al. 2009; Mucciarelli et al. 2021, and references therein). This makes them a promising way to gauge the evolution of galaxies over their lifetimes (Kissler-Patig 2000). The properties of GC systems as a whole have a remarkable story to tell in this context. The number of GCs (N_{GC}) in a system allow us to make an estimate of the GC system mass (M_{GC}) (e.g. McLaughlin & van der Marel 2005; Spitler & Forbes 2009), which is found to follow tight scaling relations with the halo mass and total luminosity of the host galaxy. This physical link between the properties of the GC system and the host galaxy was first established by Blakeslee et al. (1997), and has grown in to

a rich topic of study using various host galaxy properties (Santiago & Djorgovski 1993; Zepf & Ashman 1993; Peng et al. 2008; Spitler & Forbes 2009; Georgiev et al. 2010; Harris et al. 2013, 2015; Hudson et al. 2014; Forbes et al. 2018b; Forbes & Remus 2018; Burkert & Forbes 2020; Beasley 2020; Eadie et al. 2022; Dornan & Harris 2023). These scaling relations suggest that GCs formed in the smallest proto-galactic building blocks (e.g. Boley et al. 2009) and therefore accurately track the assembly history of galaxies thereafter (Harris 1991; Ashman & Zepf 1998; El-Badry et al. 2019; Beasley 2020). N_{GC}, M_{GC}, the luminosity, size and colour distribution all offer insightful clues about the history of their host galaxies (Kissler-Patig 2000; Spitler & Forbes 2009; Georgiev et al. 2010; Hudson et al. 2014; Harris et al. 2017; Amorisco et al. 2018; Forbes et al. 2018b; Prole et al. 2019; Beasley 2020; Doppel et al. 2021; Trujillo-Gomez et al. 2021, and references therein).

M_{GC} is found to have an empirical, near-linear correlation with M_{200} across 7 orders of magnitude (Spitler & Forbes 2009; Georgiev et al. 2010; Hudson et al. 2014; Harris et al. 2017; Forbes et al. 2018b). Populating the $M_{GC} - M_{200}$ relation with observed galaxy data is vital to build a complete picture, however measuring the halo mass of individual galaxies is difficult and relies on kinematic data from the galaxy. A review by Courteau et al. (2014) discusses the variety and reliability of mass estimator techniques in detail. However, each of these have their own limitations (Courteau et al. 2014; Coles et al. 2014; Read et al. 2017), and often require expensive and targeted follow-up observations to determine precision

masses. The $M_{GC} - M_{200}$ relation implies that by finding the GC system mass of a galaxy, one can statistically infer the galaxy's halo mass, circumventing the difficulties associated with directly observing and measuring the halo mass; although for $N_{GC} < 15$ there is considerable scatter in the relation, with little predictive power (Burkert & Forbes 2020).

In this paper, we investigate the GC system of IC 2574, a particularly intriguing, gas-rich, nearby and relatively isolated dwarf irregular (dIrr) galaxy in the M81 system. IC 2574 has a large effective radius, $r_e = 2.7$ kpc, and a low surface brightness, $\mu_{r',0} = 22.6$ mag arcsec^{-2}, which is similar to, but more luminous than, an ultra diffuse galaxy (UDG); UDGs are known to have significant variations in their GC populations (Forbes et al. 2020).

IC 2574 is at a distance of 3.86 Mpc (Dalcanton et al. 2009) and is located in the outer regions of the M81 system; it is believed to have not undergone any recent interactions, making it unlikely to have been influenced by external tidal forces (Pellerin et al. 2012; Sorgho et al. 2020; Mondal et al. 2021). IC 2574 has experienced a constant star formation history (SFH) with an intense star-forming event that occurred 1 Gyr ago (Weisz et al. 2008). IC 2574's circular velocity (v_{max}) from Oh et al. (2011) allows us to calculate an independent measurement of its halo mass, which is rare for low mass galaxies (Forbes et al. 2018b). Thus, a search for the GC candidates of IC 2574 allows us to place another galaxy on the $M_{GC} - M_{200}$ relation and determine whether IC 2574 agrees with the observed near-linear relation (Spitler & Forbes 2009).

IC 2574 appears to host a rich GC population and based on its stellar mass it should, although this has never been assessed in detail. Georgiev et al. (1996) presented results of a GC candidate search around IC 2574, identifying 11 candidates using photographic plates, including a cluster as luminous as the unusual Milky Way (MW) GC ω Cen. It is the most luminous GC in the MW (Mackey & van den Bergh 2005) and is thought to be the remnant of a tidally stripped dwarf galaxy (Majewski et al. 2000; Hilker & Richtler 2000; Leaman 2012). It would be unexpected to find an analogue of ω Cen in IC 2574 as there is no evidence for recent mergers in this galaxy (Pellerin et al. 2012; Mondal et al. 2021); as such, this could give us insight into a possible major merger in IC 2574's early history, or alternatively help us to understand what conditions aid the peculiar efficiency of forming massive GCs in dwarf galaxies (e.g. Larsen et al. 2004; Sharina et al. 2005; Villegas et al. 2008; de Grijs et al. 2013). In the analysis by Georgiev et al. (1996), magnitudes and colours were presented for the GC candidates, but not coordinates.

For the first time since, we perform a GC candidate search around IC 2574 using deep HST/ACS imaging to establish its GC system, and validate the claims of an ω Cen-like candidate.

The outline of this paper is as follows: in Section 2 we describe where we obtained the data and outline the method of photometry, the GC candidate selection criteria and the completeness corrections, in Section 3 we present our candidate GC system and the resulting GC system-galaxy scaling relations, and finally in Section 4 we summarise our findings and discuss future work.

2 DATA AND METHODOLOGY

2.1 Data

We search for globular clusters in IC 2574 using public HST/ACS imaging from the Mikulski Archive for Space Telescopes (MAST)

Table 1. Properties of IC 2574: (a) Wenger et al. (2000), (b) Dalcanton et al. (2009); distance calculated and uncertainty propagated from distance modulus 27.93 ± 0.03, (c) Chiboucas et al. (2009), (d) Wenger et al. (2000); Cook et al. (2014), (e) Cannon et al. (2005), (f) Pasquali et al. (2008), (g) Lee et al. (2006), (h) Schlegel et al. (1998), (i) Oh et al. (2011); maximum uncertainty assumed from velocity difference (true and derived rotation velocities) due to instrument limitations and observational uncertainties. Values without references are calculated in this work. Uncertainty in M_V is propagated from uncertainty in the distance modulus and uncertainty in V (Wenger et al. 2000). Uncertainty in $\log M_{200}$ is propagated from the uncertainty in v_{max}. Uncertainty in N_{GC} is Poissonian.

Properties	Value
RA (J2000)	10:28:23.61^a
Dec (J2000)	+68:24:43.44^a
D (Mpc)	3.86 ± 0.05^b
$\mu_{r',0}$ (mag arcsec^{-2})	22.6^c
$\mu_{r',e}$ (mag arcsec^{-2})	24.0^c
r_e (kpc)	2.7^c
m_V	10.87±0.03^d
M_V	−17.06 ± 0.04
Metallicity ($Z_\odot$)	0.3^e
Inclination (deg)	63^f
PA of major axis (deg)	55^f
$\log M_*$ ($M_\odot$)	8.39^g
$E(B-V)$	0.036^h
v_{max} (km s^{-1})	77.6 ± 5.0^i
$\log M_{200}$ ($M_\odot$)	10.93 ± 0.08
N_{GC}	27 ± 5
S_N	4.0 ± 0.8

Portal from the Space Telescope Science Institute (STScI) in the F814W and F555W broadband filters (Fleming et al. 2015). Candidate GC systems have been similarly examined in HST/ACS imaging, ranging across nearby giant elliptical galaxies, spiral galaxies, dwarf spheroidals (dSph) and dIrrs, and distant unbound GCs in galaxy clusters (Forbes et al. 1997; Chandar et al. 2004; Sharina et al. 2005; Hwang & Lee 2006; Barmby et al. 2006; Nantais et al. 2010; Santiago-Cortés et al. 2010; West et al. 2011; Simanton et al. 2015; Lomelí-Núñez et al. 2022; Hazra et al. 2022), as well as with similar methods on imaging from other telescopes (Goudfrooij et al. 2003; Tudorica et al. 2015; González-Lópezlira et al. 2017; Cantiello et al. 2018).

IC 2574 is visible over three pointings that each cover a 202×202 arcsec field-of-view (FOV), depicted in a mosaic in Fig. 1 with the GC candidates shown in orange. The left pointing was obtained from program 9755 (PI: Walter 2003), and the central and right pointings from program 10605 are referred to in this paper as 10605-1 and 10605-2 respectively (PI: Skillman 2005). Table 2 outlines the observation details.

2.2 Visual Inspection

In the absence of matched filter techniques or machine learning algorithms specifically designed for the identification of GCs, visual inspection of imaging data remains a common technique for identifying these objects (Hwang & Lee 2006; Barmby et al. 2006; Nantais et al. 2010, and references therein). Visual inspection involves scrutinising the images to identify the distinct sources that exhibit the characteristics indicative of GCs. As IC 2574 is relatively nearby, its GCs are resolved in size, but the individual stars are not resolved. This means they appear as compact and round partially extended ob-
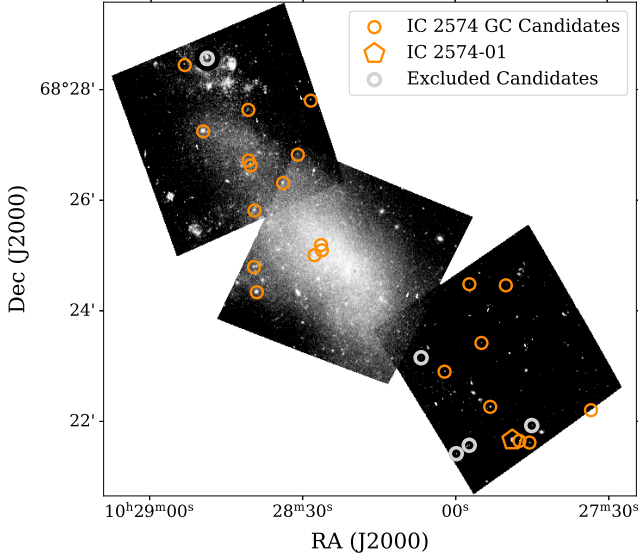
Figure 1. Mosaic of IC 2574 pointings with the distribution of GC candidates overlaid in orange circles (highest luminosity candidate IC 2574-01 is an orange pentagon). In light grey circles we have 5 excluded candidates that we speculate could be young star clusters, not GCs. From left to right we label the pointings: 9755 (East), 10605-1 (Central), 10605-2 (West), as North is up and East is to the left. Weisz et al. (2008) found that young blue stars are distributed across the galaxy (including the southern part of the West field), with the highest concentration in the northern part of the East field. Old red stars are elliptically distributed with a major axis in the northeast-southwest direction, with the highest concentration in the overlap region between the East and Central field.

Table 2. Observation log details for the three pointings; (a) Walter (2003), (b) Skillman (2005).

	9755^a [East]	10605-1^b [Central]	10605-2^b [West]
Name	IC2574-SGS	IC-2574-1-COPY	IC-2574-2
RA, Dec (J2000)	10:28:43.17,	10:28:23.07,	10:27:50.00,
	+68:27:04.56	+68:24:36.00	+68:22:54.99
Observation Date	2004-02-06	2006-03-20	2006-01-27
Exposure Time (s)	6400.0	4784.0	4784.0

jects, where only their outermost stars can be resolved around the full edge of the clusters. This makes their appearance discernible from individual stars, clusters of stars or galaxies. Visual inspection of the candidates does impart subjectivity to the selection procedure that cannot have a well-defined completeness estimate, but detailed analysis of the individually selected candidates aids in the final selection (Barmby et al. 2006; Nantais et al. 2010).

We use SAOImage DS9 (Smithsonian Astrophysical Observatory 2000; Joye & Mandel 2003) to visually inspect the images in the deeper F814W filter to find circular objects that have stars resolved around the edges, and that importantly maintain their circular shape across varying contrasts; objects found to have non-circular shapes at extreme contrasts are dismissed from consideration. We scan across all areas of each pointing image in DS9 to visually select 28 candidates based on these distinctive features. The next step is to obtain

Table 3. The input parameters for the Source Extractor runs.

Input Parameter	
DETECT_MINAREA	5
DETECT_THRESH	1.4
BACK_SIZE	32
BACK_FILTERSIZE	3
PIXEL_SCALE	0.05
PHOT_FLUXFRAC	0.5
BACKPHOTO_TYPE	LOCAL

the photometry for these candidates in order to check whether their size and colour are in line with those expected for GCs.

2.3 Photometry

To evaluate the photometry of our selected candidates, we perform source detection and aperture photometry using `Source Extractor` (SE) (Bertin & Arnouts 1996). We use SE in dual image mode with the F814W filter as the detection image, cycling through with the F814W and F555W filters as the measurement images. Using the input parameters in Table 3, as in Lomelí-Núñez et al. (2022) and following techniques from Holwerda (2005), we run SE from the command line, selecting the output parameters `FLUX_BEST`, which is useful for well-resolved sources that do not have a complex morphology, the J2000 coordinates `ALPHA_J2000` and `DELTA_J2000` and the `FLUX_RADIUS` set to 0.5, which corresponds to the half-light radius (r_h) of the source[1].

Each pointing has varying levels of crowding, therefore it is important to account for background subtraction in a more accurate way unique to each source. Setting `BACKPHOTO_TYPE` to LOCAL calculates a local background estimation in an annulus around each source, which is far more accurate in this context than otherwise using the GLOBAL background subtraction that consists of an average value across the entire image, leading to inaccurate photometry.

For the extinction correction of the fluxes, we use the extinction ratios $A(P) / E(B - V)$ of 1.825 and 3.177 for F814W and F555W respectively, as outlined in Table 14 of Sirianni et al. (2005); we use the spectral energy distribution G2, which is an appropriate choice for HST/ACS photometry because they are similar to that of the typical stars we find in GCs, as in e.g. Galleti et al. (2006). We take the extinction value $E(B - V) = 0.036$ for IC 2574 from the NASA/IPAC Infrared Science Archive (Schlegel et al. 1998), which gives us $A_{F814W} = 0.0657$ and $A_{F555W} = 0.114$. To convert the fluxes to apparent magnitudes, we use the zeropoints (ZP) for the ACS Wide Field Channel (WFC) in ABMAG in Table 10 of Sirianni et al. (2005) in the magnitude equation

$$m_{\text{filter}} = -2.5 \times \log_{10}(\text{flux}) + ZP; \qquad (1)$$

where $ZP_{F814W} = 25.937$ and $ZP_{F555W} = 25.718$. To then convert the apparent magnitudes to absolute magnitudes, we use the IC 2574 dereddened distance modulus of 27.93 ± 0.03 mag (Dalcanton et al. 2009).

For the GC selection criteria, colour cuts have been performed in the filters V and I (e.g. Forbes et al. 1997; Goudfrooij et al. 2003; Chandar et al. 2004; Sharina et al. 2005; West et al. 2011; Simanton

---

[1] When selecting `FLUX_RADIUS` in the "`-.param`" file, comment out the description line that follows it in order to avoid a syntax error.

et al. 2015), so we perform standard filter transformations from our WFC filters on the HST/ACS to the Johnson-Cousins BVRI system as outlined in Sirianni et al. (2005) using the coefficients in Table 18 in the 'observed' panel. The observed coefficients are determined from observations of standard stars and tend to be more reliable for accurate photometry in the WFC and BVRI filter systems than the synthetic coefficients. This filter transformation is performed using Equation 12 in Sirianni et al. (2005).

2.4 Globular Cluster Selection

For the final selection of our GC candidates, we apply broad cuts to our dataset in size and colour. We adopt a generous colour-cut of $0.3 \leq V - I \leq 2.0$ as in Goudfrooij et al. (2003). The HST/ACS pixel scale is 0.05 arcsec/pixel, so the projected spatial resolution for the IC 2574 distance (3.86 Mpc) is 0.935 pc/pixel. Objects found to have sizes below ~1 pc were dismissed as likely point sources (stars) based on the resolution of HST/ACS, increasing the likelihood of identifying genuine GCs and reducing the contamination of false positives caused by these individual stars or compact clusters of stars; above this 1 pc size, all GC candidates are resolved in size. Our smallest candidate is ~1.4 pc, well above this 1 pc lower limit we have defined. We expect some candidates are significantly more extended than others, so we set our upper limit size cut to an extremely extended 30 pc, consistent with extended clusters seen in Andromeda (Huxor et al. 2005).

After applying these cuts, we find 23 GC candidates, which need to be corrected for observational incompleteness. The 5 candidates that fall outside of the cuts are referred to from here on as the 'excluded candidates'; these excluded candidates have appropriate sizes but are too blue in colour to be considered GC candidates.

2.5 Completeness Corrections

There are two sources of incompleteness that we must consider in our analysis; the radial distribution and the magnitudes of the GC candidates.

We first consider the radial distribution of the GC candidates around IC 2574. In Fig. 2 we plot the radial profile of the GC candidates, i.e. N_{GC} per unit area (Σ) as a function of their distance from the centre of the galaxy (see Table 1 for central coordinates). From Fig. 1 we can see that there is good coverage along the major axis, however the incompleteness arises in the direction of the minor axis as this is only covered by one pointing across. We perform curve fitting of the GC radial profile from 0 to 3.37 arcmin (ACS FOV: 202×202 arcsec) as this is the extent of the completeness in the minor axis direction. We use the method outlined in Martin et al. (2016), where we assume that our GC system's radial distribution follows the same behaviour as would be expected for the stellar distribution of a galaxy:

$$\rho_{\mathrm{dwarf}}(r) = \frac{1.68^2}{2\pi R_{\mathrm{GC}}^2(1-\epsilon)} N_{\mathrm{GC}} \exp\left[\frac{-1.68r}{R_{\mathrm{GC}}}\right], \tag{2}$$

where we substitute N_* and r_h in the literature for our current value of $N_{\mathrm{GC}} = 23$ and fit for R_{GC} which is a scale radius that tells us the radius at which half the number of GCs per arcmin^2 are found, and where r is the elliptical radius such that:

$$r = \left[\left(\frac{1}{1-\epsilon}((x-x_0)\cos\theta - (y-y_0)\sin\theta) \right)^2 + \left((x-x_0)\sin\theta - (y-y_0)\cos\theta \right)^2 \right]^{\frac{1}{2}}. \tag{3}$$

In this equation, θ is the position angle (PA) of the major axis, x_0 and y_0 are the central coordinates of IC 2574 and x and y are the coordinates of the GC candidate. We assume that the GCs tend towards a spherical distribution, and set the ellipticity ϵ to 0.

This curve fit agrees exceptionally well with the GC radial profile and shows the farthest GCs almost reaching $\Sigma = 0$ arcmin^{-2}, which indicates that the radial completeness corrections are not substantial. In order to apply the corrections, we integrate under the curve from 0 until the maximum radial distance of GCs (12.8 arcmin), and then from this maximum to a distant 30 arcmin, where we approximate $\Sigma = 0$ arcmin^{-2} has been approached. We obtain the ratio between these two integrals to obtain the radial completeness correction, which we factor in with the magnitude completeness correction below.

We perform completeness corrections in magnitude using the GC luminosity function[2] (GCLF), as in e.g. Richtler (2003); Beasley (2020). We use the more luminous half of the GCLF, above the peak, and reflect this side to create a mirrored distribution that accounts for low-luminosity GCs that may have been missed, especially in the crowded central region of IC 2574. We fit a Gaussian distribution to the original GCLF and the mirrored GCLF, and integrate under the curve for each, using the ratio between these integrals to multiply and scale up N_{GC}.

Accounting for both the radial and magnitude completeness corrections gives us a completeness-corrected value of $N_{\mathrm{GC}} = 27 \pm 5$, including its Poissonian uncertainty, which we use for all subsequent analysis.

3 RESULTS AND DISCUSSION

3.1 The GC System

A compilation of the cutouts for all 23 GC candidates identified are shown in Fig. 3. Our candidate GCs have luminosities spanning the range $-5.9 \geq M_V \geq -10.4$. Our highest luminosity GC candidate (IC 2574-01) has $M_V = -10.4$, comparable to ω Cen (Harris 2010). The sizes of our GC candidates range from $1.4 \leq r_h \leq 11.5$ pc, with colours in the range $0.52 \leq V - I \leq 1.59$, typical of GCs (e.g. Forbes et al. 1997; Goudfrooij et al. 2003; Chandar et al. 2004; Sharina et al. 2005; Santiago-Corté s et al. 2010; Lomelí-Núñez et al. 2022). Our most extended GC candidate (IC 2574-07) has a size of 11.5 pc. The excluded candidates that were in the initial visual selection fell outside of the broad cuts because of their extremely blue ($V - I < -0.5$) colour, these are shown in Fig. 4. These objects can be seen to have similar morphological characteristics to our final GC candidates in Fig. 3.

We plot the well-known relation between the size and luminosity of our GC candidates in Fig. 5, with GCs from the MW and the dIrr Large Magellanic Cloud (LMC) plotted for comparison (Harris 2010; McLaughlin & van der Marel 2005). We overplot the relationship log

---

[2] See Sec. 3.3 for a description of the GCLF.
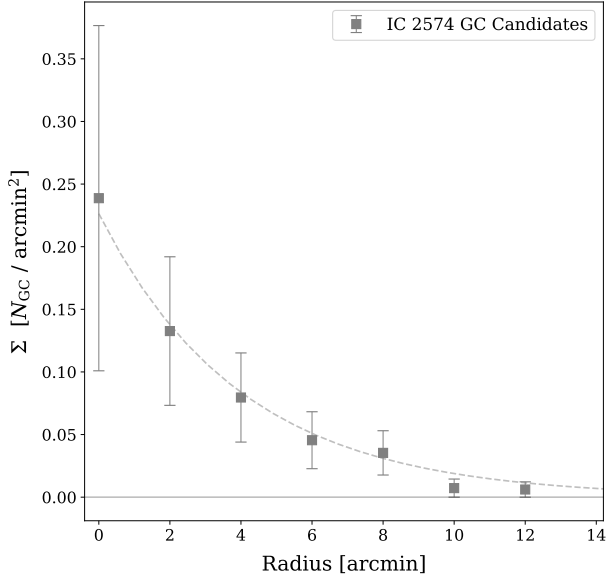
Figure 2. The radial profile of the candidate GCs of IC 2574, which shows the number of GCs per unit area (Σ) as a function of the distance from the centre in arcmin. Error bars in Σ are Poisson uncertainties. We have candidates out to 12.8 arcmin. The curve fit is applied only to the first 3.37 arcmin of data as this is the extent of our radial completeness in the minor axis direcion, which is one pointing across (ACS FOV width). We extend the curve fit out to 30 arcmin to approximate where it approaches $\Sigma = 0$ arcmin^{-2} (solid grey line). The ratio between the integrals under the curve from 0 to 12.8 arcmin and 12.8 to 30 arcmin are used to calculate the radial completeness correction (see text for details).

$r_h = 0.2 \, M_V + 2.6$ from van den Bergh & Mackey (2004), depicting a characteristic envelope typically traced by MW GCs (Mackey et al. 2013). This relation illustrates that larger GCs are intrinsically less luminous, more luminous GCs tend towards being more compact, and typically, few GCs rise above this envelope. An exception to this rule is found by van den Bergh & Mackey (2004) in the GC NGC 2419, who suspect that it could be the surviving core of a dSph galaxy, much like suggestions that ω Cen is also the surviving core of a disrupted dwarf galaxy (Majewski et al. 2000; Hilker & Richtler 2000; Bekki & Freeman 2003; Youakim et al. 2023, and references therein). We find that IC 2574-01 is in close proximity to ω Cen on this plane, suggesting it could be similar in nature to ω Cen. We also have 4 other GC candidates that lie just above the relation, which is intriguing. Interestingly, the GCs of IC 2574 are on average larger than those of the MW and LMC. Several works have shown that dwarfs, such as ScI-dE1, Fornax, NGC 6822, IKN, and Sagittarius, may host more extended clusters owing to a weaker tidal field than higher mass galaxies (Da Costa et al. 2009; Georgiev et al. 2009; Harris 2010; Hwang et al. 2011; Cole et al. 2012; Veljanoski et al. 2015; Tudorica et al. 2015; Orkney et al. 2019). IC 2574's GC system could contribute to this valuable literature if we can confirm the GCs as members of IC 2574 with spectroscopy and make a statistically significant comparison.

The 5 light grey data points (triangle symbols) in the size-luminosity plot in Fig. 5 are the excluded candidates. They have appropriate sizes as can be seen in this distribution, however the colour distribution in Fig. 6 shows that they have extremely blue

colours ($V - I < -0.5$), well below the generous lower boundary of the colour cut ($V - I = 0.3$). It is possible that these 5 excluded candidates could be young massive star clusters, because of their morphology and the extremely blue colour that they exhibit (Portegies Zwart et al. 2010). Young massive star clusters are known to form in a variety of starburst environments (Meurer et al. 1995; Watson et al. 1996), consistent with the recent intense burst of star formation that occurred in IC 2574 ~1 Gyr ago (Weisz et al. 2008). The recent burst accounts for 15% of the stars formed, which may be consistent with the fraction of excluded candidates (potential young star clusters) to all candidate clusters found, which is ∼ 16%.

### 3.2 Colour Bimodality in the GC System of IC 2574

The colour distribution of the 23 GC candidates, as well as the 5 excluded candidates, is shown in Fig. 6. For the IC 2574 GC candidates (dark grey) there appears to be a bimodal feature, which we fit with a double Gaussian. We find 30% localised around the redder $V - I = 1.5 \pm 0.1$ ($\sigma = 0.1 \pm 0.1$) and 70% around the bluer $V - I = 0.84 \pm 0.05$ ($\sigma = 0.18 \pm 0.05$). The redder GC candidates are spatially distributed across the full major axis of the galaxy, which reassures us that their redder colour is an intrinsic property and is likely not a systematic reddening effect (implied if they were centrally located). We also plot the $V - I$ bimodal colour distribution of the MW GCs (Harris 2010) in Fig. 6 to emphasise the bimodal feature exhibited by IC 2574. We scaled down the histogram height of the MW GCs by a factor of 4 to make a sensible visual comparison.

Colour bimodality is a significant characteristic of a GC system (Zepf & Ashman 1993; Gebhardt & Kissler-Patig 1999; Larsen et al. 2001), understood to be a proxy for an underlying bimodality in metallicity (Kissler-Patig et al. 1998; Brodie & Strader 2006; Chies-Santos et al. 2012; Fahrion et al. 2020; Harris 2023; Hartman et al. 2023). A metallicity bimodality is often interpreted as a signature of distinct formation channels within a GC system (Harris & Pudritz 1994; Meurer et al. 1995; Watson et al. 1996; Forbes et al. 1997; Côté 1999; Larsen et al. 2001; Brodie & Strader 2006; Kruijssen 2014; Choksi & Gnedin 2019; Reina-Campos et al. 2022), e.g. those formed in-situ and those accreted onto the galaxy (Zepf & Ashman 1993; Forbes et al. 1997; Gebhardt & Kissler-Patig 1999; Larsen et al. 2001; Kundu & Whitmore 2001; Peng et al. 2006; Brodie & Strader 2006; Lomelí-Núñez et al. 2022). The MW and M81 GC systems are examples of galaxies exhibiting bimodal colour and confirmed intrinsic bimodal metallicity distributions (Côté 1999; Perrett et al. 2002; Chandar et al. 2001; Ma et al. 2005; Nantais et al. 2010; Santiago-Corté s et al. 2010; Nantais et al. 2011).

As such, IC 2574's bimodal colour distribution could suggest two subpopulations with different formation mechanisms or alternatively an in-situ population and an accreted metal-poor GC population from a lower mass galaxy. Although IC 2574 has no signs of present interaction, there is the possibility of a past merger as dwarf-dwarf mergers have been observed (e.g. Rich et al. 2012; Martínez-Delgado et al. 2012), simulated and discussed in the literature (Forbes & Bridges 2010; Deason et al. 2014; Wetzel et al. 2015; Wheeler et al. 2015; Deason et al. 2015). The presence of two different metallicity populations would require confirmation with spectroscopy of the IC 2574 GCs.

3.3 The GC Luminosity Function

The GC luminosity function is a robust and predictable feature of a galaxy's GC system (Harris 1991). The GCLF is expected to exhibit
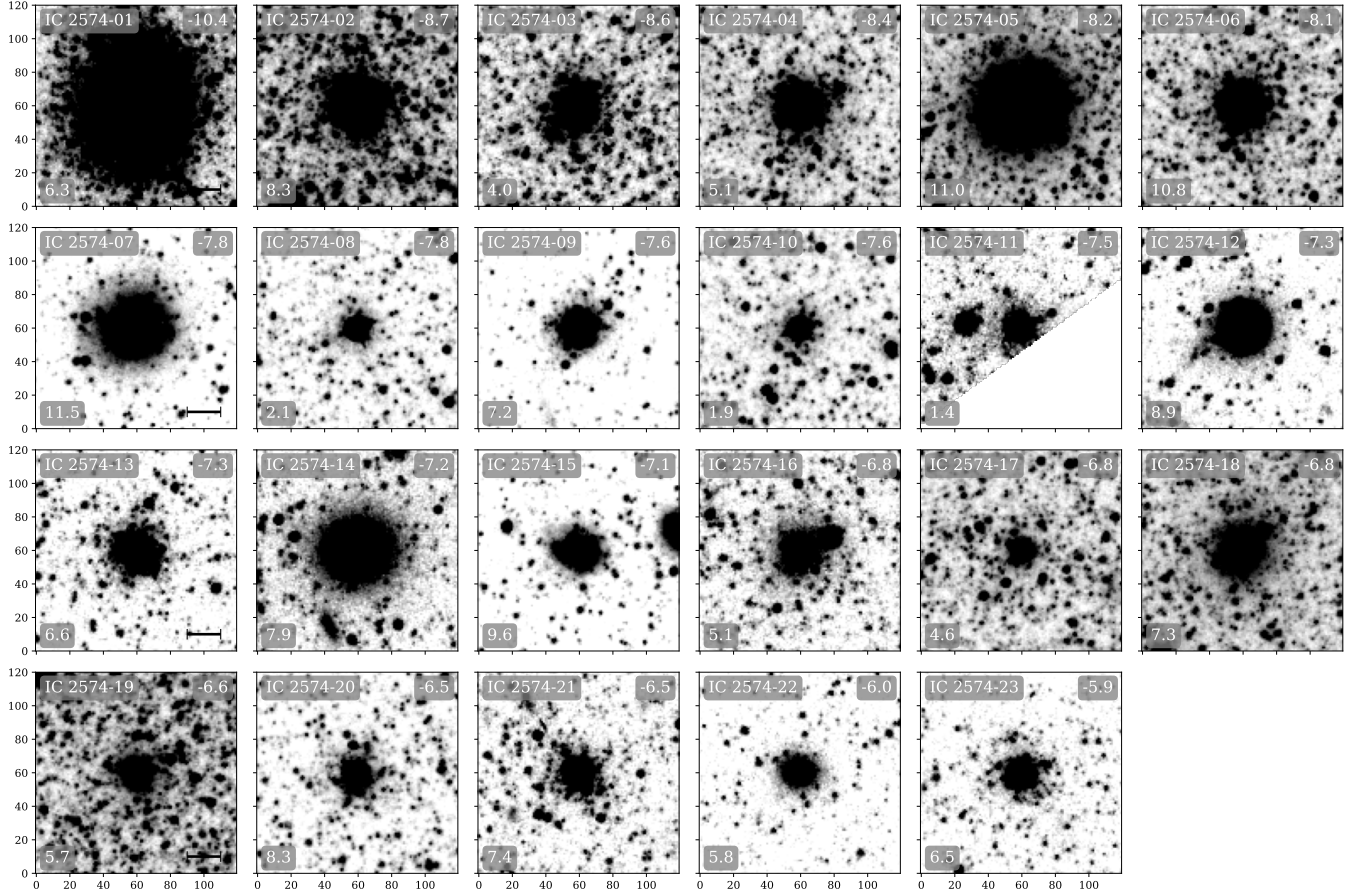
Figure 3. Globular cluster candidates of IC 2574 ordered by M_V. All cutout images are centred on the candidates in a 120×120 pixel box, with the GC candidate name in the top left, M_V in the top right and r_h in the bottom left in pc. The bar in the bottom right of the first column of cutouts indicates 1" in the image. North is up, East is to the left.
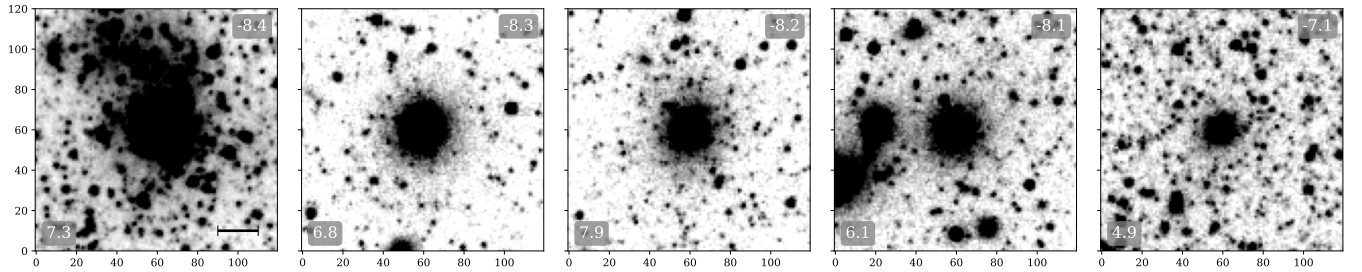
Figure 4. The 5 excluded candidates that do not pass the cuts outlined in Sec. 2.4, ordered by M_V. All cutout images are centred on the object in a 120×120 pixel box, with M_V in the top right and r_h in the bottom left in pc. The bar in the bottom right of the first cutout indicates 1" in the image. These 5 objects are also shown in Fig. 5 and Fig. 6 as light grey data points; these are dismissed from the final GC candidate selection as although they are within the size cut, they fall beyond the colour cut with extra blue colour. We speculate that these could be young star clusters given their extremely blue colour. North is up, East is to the left.

a log-normal distribution, typically centred around a turnover (TO) magnitude of $M_{V,\mathrm{TO}} \sim -7.5$, with the GCLF dispersion systematically widening with increasing galaxy luminosity (e.g. Secker 1992; Reed et al. 1994; Whitmore et al. 1995; Harris 1996; Bica et al. 2006; Richtler 2003; Jordán et al. 2007; Villegas et al. 2010; Peacock et al. 2010; Harris et al. 2014; Forbes et al. 2018a), with evidence that the

TO magnitude can be less luminous ($M_{V,\mathrm{TO}} \sim -7.3$) for low-mass galaxies (Miller & Lotz 2007).

We present the GCLF for IC 2574 in Fig. 8, which exhibits the expected features of a log-normal distribution centred around $M_{V,\mathrm{TO}}$. To find $M_{V,\mathrm{TO}}$, we employ a Markov Chain Monte Carlo (MCMC) routine with emcee (Foreman-Mackey et al. 2013) to fit a Gaussian distribution to the GCLF. The MCMC routine is a robust approach to

Table 4. A catalogue of the GC candidate properties: the RA, Dec coordinates in J2000, the $V - I$ colour, the absolute magnitude M_V, the half-light radius r_h in pc and its field. All r_h values are assumed to have an uncertainty of 0.5 pc, accounting for the limitations in instrument resolution. The uncertainties for all colour values are 0.02 mag and the uncertainties for the M_V values are 0.1 mag; the uncertainties are propagated through from the uncertainties in the flux obtained from `Source Extractor`, the filter transformations and the distance to IC 2574. The bottom section of the table has the same information for the 'excluded' candidates that could be young massive star clusters (YMC).

| Name	RA (J2000)	Dec (J2000)	V-I	M_V	r_h (pc)	Field
IC 2574-01	10:27:48.90	+68:21:40.30	0.83	-10.4	6.3	10605-2
IC 2574-02	10:28:26.44	+68:25:11.86	0.69	-8.7	8.3	10605-1
IC 2574-03	10:28:27.70	+68:25:00.86	0.89	-8.6	4.0	10605-1
IC 2574-04	10:28:33.93	+68:26:19.05	0.90	-8.4	5.1	9755
IC 2574-05	10:28:49.64	+68:27:15.01	1.53	-8.2	11.0	9755
IC 2574-06	10:28:40.32	+68:26:38.07	0.68	-8.1	10.8	9755
IC 2574-07	10:28:39.05	+68:24:20.59	1.41	-7.8	11.5	10605-1
IC 2574-08	10:28:31.02	+68:26:49.89	1.07	-7.8	2.1	9755
IC 2574-09	10:28:28.46	+68:27:48.53	0.80	-7.6	7.2	9755
IC 2574-10	10:28:40.78	+68:27:38.47	1.44	-7.6	1.9	9755
IC 2574-11	10:27:33.44	+68:22:12.26	1.59	-7.5	1.4	10605-2
IC 2574-12	10:27:45.53	+68:21:37.29	0.99	-7.3	8.9	10605-2
IC 2574-13	10:27:47.50	+68:21:39.19	0.52	-7.3	6.6	10605-2
IC 2574-14	10:27:53.22	+68:22:16.14	1.48	-7.2	7.9	10605-2
IC 2574-15	10:28:39.61	+68:24:47.96	1.10	-7.1	9.6	10605-1
IC 2574-16	10:28:02.17	+68:22:54.39	1.02	-6.8	5.1	10605-2
IC 2574-17	10:28:40.75	+68:26:43.55	0.86	-6.8	4.6	9755
IC 2574-18	10:28:39.52	+68:25:49.22	1.54	-6.8	7.3	9755
IC 2574-19	10:28:26.28	+68:25:06.09	1.45	-6.6	5.7	10605-1
IC 2574-20	10:28:53.32	+68:28:27.01	0.70	-6.5	8.3	9755
IC 2574-21	10:27:54.92	+68:23:25.49	0.76	-6.5	7.4	10605-2
IC 2574-22	10:27:50.10	+68:24:27.95	0.97	-6.0	5.8	10605-2
IC 2574-23	10:27:57.27	+68:24:29.27	0.70	-5.9	6.5	10605-2
IC 2574-YMC-01	10:28:48.90	+68:28:34.30	-0.65	-8.4	7.3	9755
IC 2574-YMC-02	10:27:59.89	+68:21:25.39	-0.65	-8.3	6.8	10605-2
IC 2574-YMC-03	10:27:45.07	+68:21:55.79	-0.84	-8.2	7.9	10605-2
IC 2574-YMC-04	10:27:57.34	+68:21:34.50	-0.75	-8.1	6.1	10605-2
IC 2574-YMC-05	10:28:06.76	+68:23:09.50	-0.82	-7.1	4.9	10605-2

explore the parameter space and estimate the optimal values for the mean ($M_{V,\mathrm{TO}}$) and standard deviation (σ_{GCLF}) of the raw, unbinned data. We find $M_{V,\mathrm{TO}} = -7.5 \pm 0.2$ and $\sigma_{\mathrm{GCLF}} = 1.0 \pm 0.2$, not dissimilar to the mean values from the sample of dIrr galaxies in Georgiev et al. (2009, $M_{V,\mathrm{TO}} = -7.56 \pm 0.02$, $\sigma_{\mathrm{GCLF}} = 1.23 \pm 0.03$). A scaled Gaussian distribution with our $M_{V,\mathrm{TO}}$ and σ MCMC values is plotted over the GCLF in Fig. 8.

A distinct feature in IC 2574's GCLF is the highest luminosity GC candidate, IC 2574-01. With $M_V = -10.4$, it is comparable in luminosity to ω Cen ($M_V = -10.3$, Harris 2010). The presence of massive clusters is noteworthy in dwarf galaxies, such as young and similarly massive clusters in nearby starburst dwarfs like NGC 1569 (Ho & Filippenko 1996), NGC 5253 (de Grijs et al. 2013), NGC 4449, NGC 4214 (Larsen et al. 2004), II Zw 40 (Beck et al. 2002) and WLM (Hodge et al. 1999), with some showing signs of mergers. Since IC 2574 has no evidence of recent mergers (Pellerin et al. 2012; Sorgho et al. 2019; Mondal et al. 2021), the total disruption of a dwarf galaxy massive enough to possess a nuclear star cluster would be surprising, although we do see nuclear clusters in very low-mass dwarfs (van Dokkum et al. 2018b, 2019a). Massive clusters can also be formed in dense regions of galaxy clusters (van den Bergh 2001), however given the relatively isolated nature of IC 2574, the alternative is that an intense star formation event (Weisz et al. 2008) could be responsible for the creation of this massive ω Cen-like

GC in its gas-rich environment. Spectroscopic follow-up of the GCs would allow us to determine the chemistry and age of each cluster, providing stringent constraints on GC formation models (Forbes et al. 2018a), and allow us to constrain the nature of IC 2574-01. The stable conditions within the relatively isolated IC 2574 may be key to understanding the formation and survival of such massive clusters.

At the opposite end, we see that the GCLF does not extend all the way to the typically lowest luminosity values for GC systems (Pan et al. 2022; Bonatto & Bica 2008; Crnojević et al. 2016; Caldwell et al. 2017). This is likely due to either photometric incompleteness for low-luminosity, diffuse clusters, or GC destruction. Completeness corrections in magnitude for the low-luminosity end of the GCLF were performed in Sec. 2.5, and increase the number of GCs to the corrected N_{GC} count by 3. An alternative is that the low-luminosity end of the GCLF can be influenced by the destruction of GCs within the galaxy by internal dynamical processes over long timescales (see: Barmby et al. 2001; Fall & Zhang 2001; Carlson & Holtzman 2001). These dynamical effects are strongest towards the centre of the galaxy. High density gas present during intense star formation episodes can also destroy GCs (Kruijssen et al. 2012), which is relevant for IC 2574 as it recently experienced an intense burst of star formation 500 Myr − 1 Gyr ago (Weisz et al. 2008; Pasquali et al. 2008). The enhanced tidal interactions from this dense gas-rich environment could contribute to the disruption and dissolution of
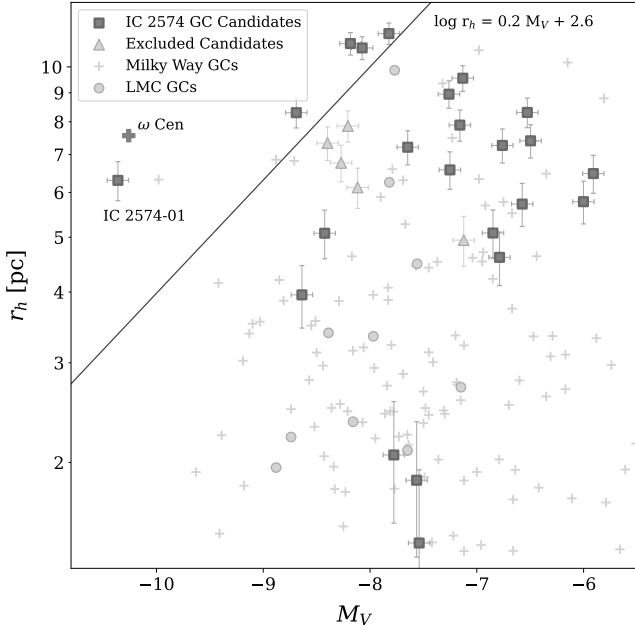
Figure 5. The relation between the size r_h (pc) and luminosity M_V of our GC candidates. The GC candidates do not spread across the r_h vs. M_V plane uniformly but tend to abide by the relation $\log r_h = 0.2 M_V + 2.6$ (solid line), that sets an envelope that is typically traced by GCs (van den Bergh & Mackey 2004; Mackey et al. 2013). This relation illustrates that larger GCs are intrinsically less luminous, more luminous GCs tend towards being more compact, and typically GCs do not rise above this envelope. The MW GC ω Cen is a known exception to this rule (lying above the boundary), which is plotted on this distribution (labelled bold plus symbol) with a more recent r_h value from Evans et al. (2022). All of the other MW GCs from the Harris (2010) catalogue are plotted as light grey plus symbols. We also plot selected LMC GCs from McLaughlin & van der Marel (2005) as light grey circles for a dwarf system comparison. IC 2574-01 is also a clear exception to this rule, situated close to ω Cen, well beyond the boundary of the envelope; it is plausible that our ω Cen-like candidate is similar in nature. We also have 4 other GC candidates that lie just above the relation, these further exceptions could suggest a unique story about the formation of IC 2574's GC system.

lower luminosity GCs, as opposed to higher luminosity GCs that tend to be higher mass and dense, making them less susceptible to disruption from their environment (Richtler 2003). A third possible alternative is that IC 2574 only contains a total of 27 GCs and sampling effects have led to the absence of some lower luminosity GCs.

### 3.4 The Specific Frequency of GCs in IC 2574

Harris & van den Bergh (1981) defined the GC specific frequency (S_N) of a galaxy as the GC formation efficiency, N_{GC} per unit galaxy luminosity, allowing us to compare N_{GC} of different galaxies by normalising it to a galaxy with luminosity $M_V = -15$. It is defined as

$$S_N = N_{GC} \times 10^{0.4(M_V+15)}, \tag{4}$$

where M_V is the absolute V−band magnitude of the host galaxy. IC 2574 has an apparent V-band magnitude of $V = 10.87 \pm 0.03$ (Wenger et al. 2000; Cook et al. 2014), giving $M_V = -17.15 \pm 0.04$.
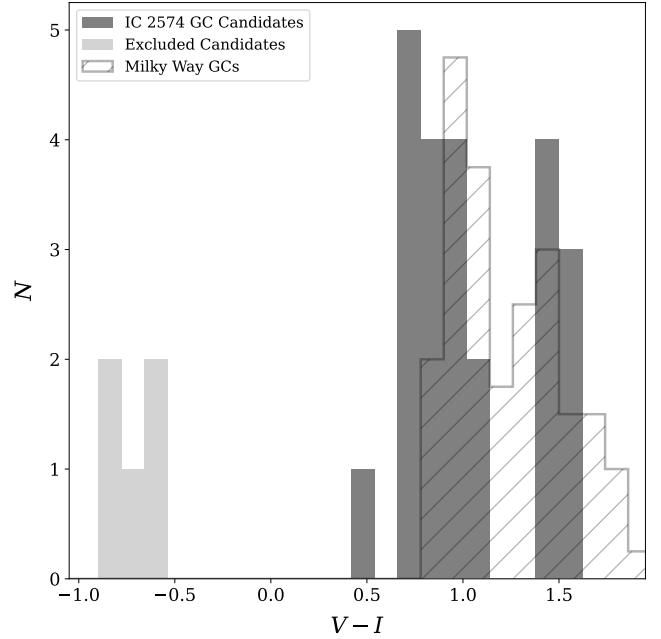

Figure 6. The colour distribution of the 23 candidate GCs of IC 2574 (dark grey), which appears to exhibit a bimodal feature. We plot the $V - I$ colour distribution of the MW GCs (Harris 2010) with a height scaled down by a factor of 1/4 to emphasise the apparent colour bimodality of the IC 2574 GC candidates in comparison to the MW GCs. On the far left with the extremely blue colours are the 5 excluded candidates that fall outside of the $0.3 \leq V - I \leq 2.0$ colour cut (light grey), which could potentially be young star clusters linked to the recent star formation that occurred in IC 2574 ~1 Gyr ago.
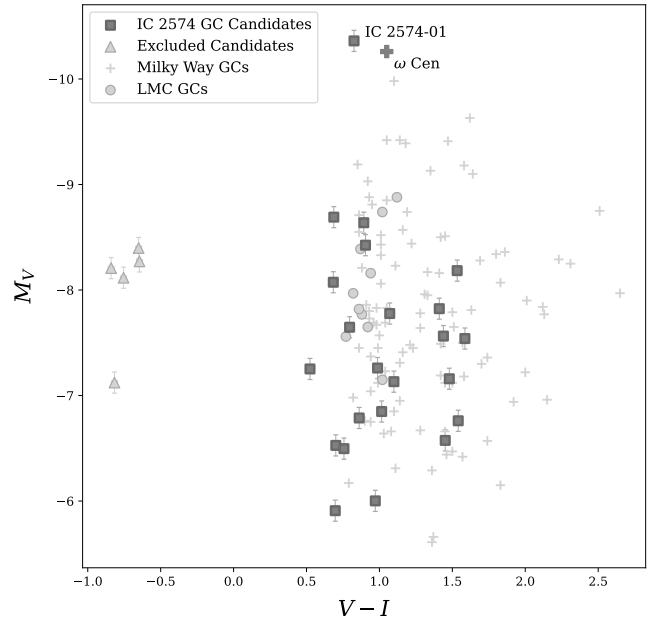
Figure 7. The colour-magnitude diagram, with $V - I$ vs. M_V, for our GC candidates and excluded candidates. We plot the Milky Way GCs (Harris 2010) and selected LMC GCs (McLaughlin & van der Marel 2005) for comparison.
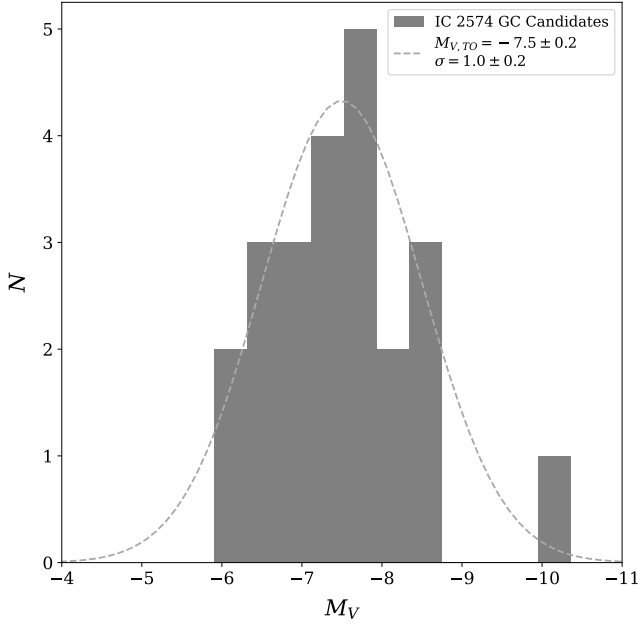
Figure 8. The luminosity function of the GC candidates for IC 2574, spanning a range $-5.9 \geq M_V \geq -10.4$, with a turnover magnitude of $M_V = -7.5 \pm 0.2$ and standard deviation $\sigma = 1.0 \pm 0.2$; scaled Gaussian fit overlaid. The highest luminosity candidate, IC 2574-01, has $M_V = -10.4$.

We use $N_{\rm GC} = 27 \pm 5$ to calculate a value for its GC specific frequency of $S_N = 4.0 \pm 0.8$; the error is propagated from M_V and the Poissonian uncertainty in $N_{\rm GC}$.

Galaxy morphology, environment, SFH and luminosity are all factors to consider for S_N (Harris & van den Bergh 1981; Peng et al. 2008; Harris et al. 2013; Lim et al. 2018). Fig. 9 shows the relation between S_N and M_V with the galaxy catalogue from Harris et al. (2013) and IC 2574 overlaid. The key feature of this relation is the distinct U-shaped distribution, discussed extensively in Forbes (2005), Peng et al. (2008) and Georgiev et al. (2010), where galaxies with intermediate luminosities gather tightly in the 'valley' of the distribution which occurs around $S_N \simeq 1$, with the dwarf and giant galaxies at either end scattering greatly upwards with much higher average S_N; this characteristic shape is driven by the halo mass of the galaxies and essentially the shape of the stellar mass-halo mass relation (SHMR; Wechsler & Tinker 2018; Girelli et al. 2020), as there is a near-constant $M_{\rm GC} - M_{200}$ relation and uniformity in the GCLF of the galaxies across the sample.

From Fig. 9, IC 2574 appears to have a typical S_N for its luminosity (albeit at the higher end of the range for late-type galaxies), consistent with a clear trend of other late-type dIrrs having increased S_N with decreasing luminosity (Georgiev et al. 2010). On the right of Fig. 9 we plot the related distribution of $N_{\rm GC}$ against the stellar mass, where the stellar mass for IC 2574 is $\log M_* = 8.39\,M_\odot$ (Lee et al. 2006). This shows that the $N_{\rm GC}$ of IC 2574 is on the higher end of the distribution than that of other late-type dwarfs within the same luminosity. High specific frequencies of late-type dwarfs can be attributed to bursty star formation, consistent with the recent burst seen in IC 2574 ~ 1 Gyr ago (Pasquali et al. 2008; Weisz et al. 2008). The S_N vs. M_V relation in the low-mass regime indicates that dwarf galaxies tend to have a greater fraction of their stellar mass in GCs as their luminosity decreases. One possible explanation for this trend is that dwarf galaxies with GCs are more efficient at forming

and retaining these clusters, or alternatively, they are less efficient at forming field stars. IC 2574's position on this relation demonstrates excellent agreement with the expected behaviour for a galaxy of its specific morphology and environment.

3.5 GC System-Galaxy Scaling Relations

The relationship between a GC system and its host galaxy is complex and multifaceted, requiring the study of many different aspects of both the GC system and the host galaxy itself. Here we calculate $M_{\rm GC}$ of IC 2574 by multiplying $N_{\rm GC}$ with an average GC mass of $4 \times 10^5\,M_\odot$, as in Spitler & Forbes (2009). This gives us $\log M_{\rm GC} = 7.03 \pm 0.08$. We plot IC 2574 on the GC system mass-stellar mass relation and the GC system mass-halo mass relation. These are recreated from Forbes et al. (2018b) with their Tables 1 and 2, which are Local Group dE and dSph galaxies and late-type dwarfs respectively. We also use the catalogue of galaxies from Spitler & Forbes (2009), which is dominated by early-type massive elliptical and lenticular galaxies.

3.5.1 GC System Mass-Stellar Mass Relation

We begin with the physically motivated GC system mass-stellar mass relation, shown in Fig. 10. We find that IC 2574 is consistent with what is expected from its stellar mass, lying sensibly within the boundaries in the dashed lines of Fig. 10. The boundaries represent GC system mass to galaxy stellar mass ratios of 10% and 0.01%; IC 2574 sits close to the 10% boundary, suggesting that this galaxy has efficient GC formation relative to its (field) star formation.

3.5.2 GC System Mass-Halo Mass Relation

In Fig. 11 we show the GC system mass-halo mass relation with IC 2574 overlaid. The data for other galaxies is assembled from Spitler & Forbes (2009) and Forbes et al. (2018b). The halo mass of the host galaxies from Forbes et al. (2018b) have been calculated from their kinematics. We also plot the three UDGs as in Forbes et al. (2018b); VCC 1287 (Beasley et al. 2016), DF 44 (van Dokkum et al. 2019b) and DF 2 (van Dokkum et al. 2018a). These three UDGs have stellar masses of the order $M_* \sim 10^7 - 10^8\,M_\odot$, similar to IC 2574. This spread in their position on the GC system mass-halo mass relation is interesting to note as a comparison to IC 2574, which lies on the boundary of UDG characteristics.

In order to add IC 2574 to the GC system mass-halo mass relation, we make an independent empirically derived estimate of M_{200} using its $v_{\rm max}$ of $77.6 \pm 5.0\,{\rm km s}^{-1}$ (Oh et al. 2011). We use the relations (from e.g. Sigad et al. 2000);
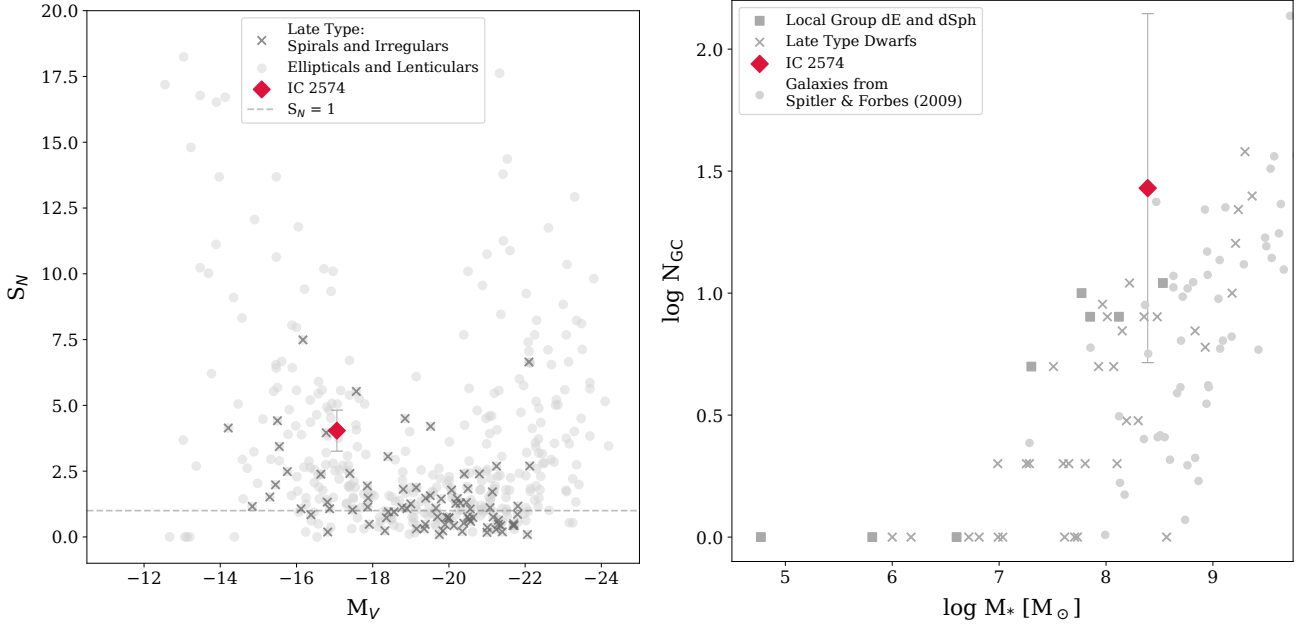
$$M_{200} = \frac{4\pi}{3} R_{200}{}^3 \times 200\,\rho_{\rm cm}, \tag{5}$$

$$V_{200} = \sqrt{\frac{G M_{200}}{R_{200}}}, \tag{6}$$

and the Navarro–Frenk–White (NFW) profile for the density distribution (Navarro et al. 1996):

$$M_{200} = 4\pi \rho_0 R_s{}^3 \left[\ln(1+c) - \frac{c}{1+c} \right], \tag{7}$$

with the concentration parameter $c = R_{200}/R_s$ (Diemer & Joyce 2019), values for c taken from Castellanos et al. (2020), and the

Figure 9. *Left*: The specific frequency S_N vs. absolute $V-$band magnitude M_V of galaxies. Cross symbols represents late-type galaxies (spirals and irregulars), and round symbols represent early-type galaxies (ellipticals and lenticulars). IC 2574 is plotted as a red diamond. Comparing IC 2574 to other late-type dwarfs (cross symbols) shows us that it is consistent with the trend of increased S_N with decreasing luminosity for dIrrs, and that it exists on the higher end of this upward turn of the distribution. *Right*: The related distribution of N_{GC} vs. M_*. Square symbols are Local Group dE and dSph and the cross symbols are late-type dwarfs from Forbes et al. (2018b). Round symbols are galaxies from Spitler & Forbes (2009), dominated by early-type massive ellipticals and lenticulars. Dwarfs for which $N_{GC} = 0$ are not included. IC 2574 is plotted as a red diamond. IC 2574 has a higher N_{GC} (and thus S_N) on this relation compared to other late-type dwarfs (cross symbols) within its luminosity band, hinting comparatively more efficient GC formation because of its unique conditions.
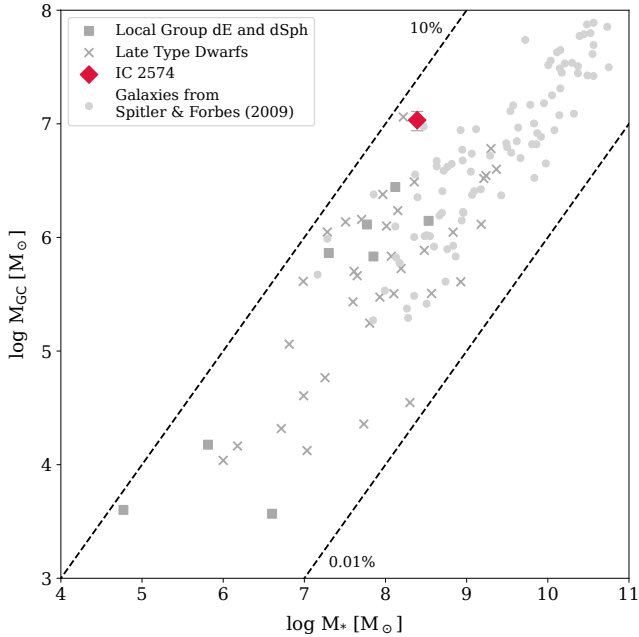
Figure 10. M_{GC} as a function of stellar mass M_* of each galaxy. IC 2574 is plotted as a red diamond. Square symbols are Local Group dE and dSph and cross symbols are late-type dwarfs from Forbes et al. (2018b), round symbols are galaxies from the Spitler & Forbes (2009) catalogue, dominated by early-type massive ellipticals and lenticulars. Dashed lines represent 10% and 0.01% ratios of M_{GC} to M_*. IC 2574 sits high on this relation, close to the 10% boundary, suggesting efficient GC formation in this galaxy.

relation $R_{max} = 2.16 \times R_s$ (Weinmann et al. 2013), to rearrange for known parameters and substitute in to the below equation (e.g. Dutton & Macciò 2014; Comparat et al. 2017),

$$v_{max} = \sqrt{\frac{GM(< R_{max})}{R_{max}}} \qquad (8)$$

where we rearrange v_{max} for M_{200}. We estimate IC 2574's halo mass as $M_{200} = (8.54 \pm 1.65) \times 10^{10} \, M_\odot$ (log $M_{200} = 10.93 \pm 0.08 \, M_\odot$), with the uncertainties propagated from v_{max}, where we assume the uncertainty stated in Table 1 is the velocity difference between the true and derived rotation velocities, which is the maximum uncertainty from limitations in the instrument.

We also calculate the value for M_{200} using the SHMR abundance matching technique from Read et al. (2017), with M_* from Table 1, finding $M_{200} = 5.2 \pm 0.4 \times 10^{10} M_\odot$ (log $M_{200} = 10.72 \pm 0.03$ $M_\odot$). While the empirical kinematic measurement and the abundance matching SHMR prediction yield M_{200} estimates that do not have overlapping uncertainty ranges, both values are well within the same order of magnitude.

Burkert & Forbes (2020) describe the relationship[3] between N_{GC} and M_{vir} as log N_{GC} = $-9.58 \, (\pm 1.58)$ + $0.99 \, (\pm 0.13) \times \log M_{vir}(M_\odot)$, where our N_{GC} = 27 ± 5 gives a value for log $M_{vir} = 11.1 \, M_\odot$, which has an uncertainty of

---

[3] This is used as an approximation since M_{vir} is not necessarily equal to M_{200}; it represents the mass enclosed within the virial radius, at which the density is equal to the critical density ρ_c of the Universe, multiplied by an overdensity constant Δ_c. If $\Delta_c = 200$, which is the typical assumption, then it becomes M_{200}.
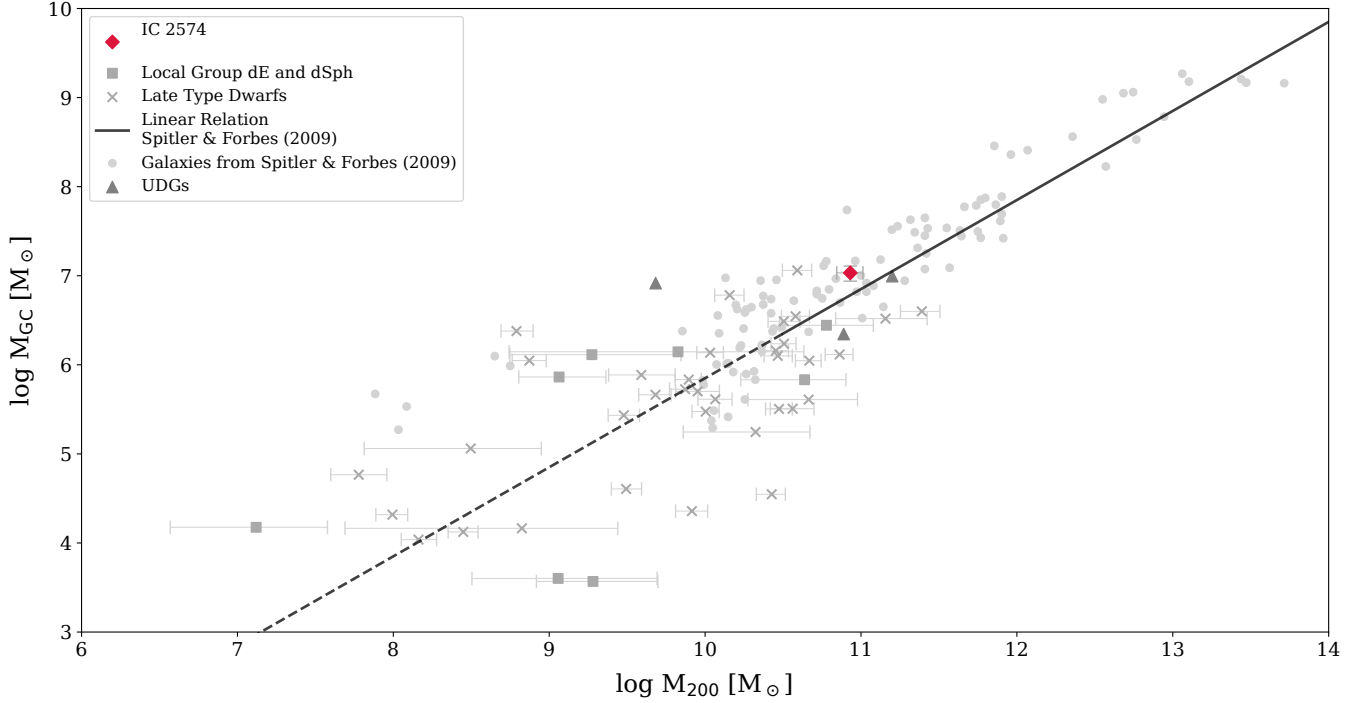
Figure 11. The GC system mass-halo mass relation, $M_{GC} - M_{200}$. Square symbols are Local Group dE and dSph, cross symbols are late-type dwarfs from Forbes et al. (2018b), round symbols are from a sample of mostly early-type massive elliptical and lenticular galaxies from Spitler & Forbes (2009). Three UDGs have been plotted as in Forbes et al. (2018b): VCC 1287 (Beasley et al. 2016), DF 44 (van Dokkum et al. 2019b) and DF 2 (van Dokkum et al. 2018a). The red diamond is IC 2574, which falls just on the $M_{GC} - M_{200}$ relation. The solid line is the linear fit from Spitler & Forbes (2009). IC 2574 has a GC system mass expected of a galaxy with its halo mass, from independent measures of both its halo mass, calculated from its kinematic data and its GC system.

0.3 dex (Burkert & Forbes 2020). This shows agreement with the empirically derived halo mass above.

We have used the empirically derived M_{200} to add IC 2574 to the $M_{GC} - M_{200}$ relation in Fig. 11. We see that IC 2574 agrees with the near-linear observed relation from Spitler & Forbes (2009), well within its scatter, which is what we would expect given the luminosity of this galaxy. If confirmed, IC 2574 does appear to have a substantial GC system. This result also agrees with simulated GC formation scenarios such as those of Chen & Gnedin (2023, and their previous works cited within), who account for the stochasticity of GC occupation in the low-mass regime, which arises from a complex interplay of baryonic effects. They predict the near-linearity of the $M_{GC} - M_{200}$ relation down to $M_{200} \simeq 10^8 M_\odot$. Chen & Gnedin (2023) also predict that more than 50% of galaxies with $M_* \leq 2 \times 10^7 M_\odot$ do not host GCs. Eadie et al. (2022) use a statistical model to find the 50% probability point for a galaxy to host GCs is $M_* \leq 10^{6.8} M_\odot$; they discuss improvements to this value by incorporating a hierarchical model to account for uncertainties in M_* (Berek et al. 2023), and ultimately the observational need to add galaxy data in and below the transition region between the observed relation ($M_{GC} - M_*$ instead, due to limitations in independent M_{200} measurements) and where galaxies appear to host no GCs. This motivates the critical next steps in building the census of galaxies in the low-mass regime with secure halo mass measurements, especially that of relatively isolated dwarfs like IC 2574 to have the effects of tidal interactions minimised on their halos and GC systems, in order to understand their GC formation efficiencies in a fundamental way. We can use similar techniques to add lower mass galaxies to this relation and test GC formation mod-

els that have made predictions to lower masses (Muratov & Gnedin 2010; Li & Gnedin 2014; Choksi et al. 2018; Chen & Gnedin 2022; Eadie et al. 2022; Chen & Gnedin 2023). Increasing this low-mass census will assess the robustness of using the GC system mass-halo mass relation as a technique for halo mass estimates, as this near-linear correlation could be evidence of universal physical processes governing GC formation and evolution in galaxies across all mass scales.

4 CONCLUSIONS

In this paper we have presented a quantitative description of the GC population of IC 2574 for the first time. We summarise our key findings below.

• We have surveyed deep HST/ACS images for IC 2574 and identified 23 candidate globular clusters for this system. After completeness corrections, we find that IC 2574 has a total GC system of $N_{GC} = 27 \pm 5$. Their luminosities range from $-5.9 \geq M_V \geq -10.4$, and their sizes are typical of GCs, spanning a range of $1.4 \leq r_h \leq 11.5$ pc.

• Our 23 candidate GCs show evidence of colour bimodality. This could suggest two distinct formation channels for these GCs. Our 5 excluded candidates exhibit extremely blue colours, which could potentially be young massive star clusters linked to the burst of intense star formation in IC 2574 ~1 Gyr ago.

• We find a very high-luminosity GC candidate in IC 2574 (IC 2574-01) that is an analogue of the unusual and rare ω Cen GC in the Milky Way. If confirmed spectroscopically, this makes

IC 2574 a notable addition to a collection of dwarfs that host high-luminosity massive GCs, and can help us understand whether it has had a significant past merger with a galaxy containing a nuclear star cluster.

- Although IC 2574 is not technically a UDG it is a fairly unusual galaxy in that it has a large effective radius and low surface brightness. This could be an interesting note in the discussion of UDGs and their high-luminosity GCs if we can confirm the membership and nature of IC 2574-01.

- We find that IC 2574's GC system is in agreement with that expected for a galaxy of its mass and morphology. It has a GC specific frequency of $S_N = 4.0 \pm 0.8$, consistent with other late-type dIrrs. It sits on the GC system mass-stellar mass distribution ($M_{GC} - M_*$) with a high ratio of ~10%, suggesting efficient GC formation relative to its (field) star formation. Its position in the N_{GC} and M_* distribution is a related illustration that demonstrates IC 2574 hosts more GCs than is typical for a galaxy of its stellar mass.

- IC 2574 experienced a recent intense burst of star formation ~1 Gyr ago that accounts for 15% of the stars formed, and which might explain the 5 extremely blue star clusters we found. These 5 objects make up 16% of the total number of candidate clusters.

- IC 2574 has a well-determined HI rotation curve, which we use to derive its halo mass and place it on the GC system mass-halo mass relation ($M_{GC} - M_{200}$). IC 2574 agrees very well with this relation, suggesting it has a fairly normal GC population in terms of the GC system mass, although it does host the unusually high-luminosity ω Cen analogue IC 2574-01.

For future work it is paramount that we confirm this population of candidate GCs with spectroscopic data to obtain their radial velocities, metallicities, estimate their ages and obtain their chemical abundance measurements. This will enable us to truly understand why the distribution of colours and sizes within the GC system are this way and build a broader picture of what happened in IC 2574 from the formation of its ancient population of GCs to its possible young star cluster formation in its recent star formation episode.

ACKNOWLEDGEMENTS

DATA AVAILABILITY

The data underlying this article will be shared on reasonable request to the corresponding author.

REFERENCES

Amorisco N. C., Monachesi A., Agnello A., White S. D. M., 2018, MNRAS, 475, 4235
Ashman K. M., Zepf S. E., 1998, Globular Cluster Systems. Cambridge University Press 1998
Astropy Collaboration et al., 2013, A&A, 558, A33
Barmby P., Huchra J. P., Brodie J. P., 2001, AJ, 121, 1482
Barmby P., Kuntz K. D., Huchra J. P., Brodie J. P., 2006, AJ, 132, 883
Bastian N., Lardo C., 2018, ARA&A, 56, 83
Beasley M. A., 2020, in , Reviews in Frontiers of Modern Astrophysics. Springer International Publishing, pp 245–277, doi:10.1007/978-3-030-38509-5_9, https://doi.org/10.1007%2F978-3-030-38509-5_9
Beasley M. A., Romanowsky A. J., Pota V., Navarro I. M., Martinez Delgado D., Neyer F., Deich A. L., 2016, ApJ, 819, L20
Beck S. C., Turner J. L., Langland-Shula L. E., Meier D. S., Crosthwaite L. P., Gorjian V., 2002, AJ, 124, 2516
Bekki K., Freeman K. C., 2003, MNRAS, 346, L11
Berek S. C., Eadie G. M., Speagle J. S., Harris W. E., 2023, ApJ, 955, 22
Bertin E., Arnouts S., 1996, A&AS, 117, 393
Bica E., Bonatto C., Barbuy B., Ortolani S., 2006, A&A, 450, 105
Blakeslee J. P., Tonry J. L., Metzger M. R., 1997, AJ, 114, 482
Boley A. C., Lake G., Read J., Teyssier R., 2009, ApJ, 706, L192
Bonatto C., Bica E., 2008, A&A, 479, 741
Brodie J. P., Strader J., 2006, ARA&A, 44, 193
Burkert A., Forbes D. A., 2020, AJ, 159, 56
Caldwell N., Strader J., Sand D. J., Willman B., Seth A. C., 2017, Publ. Astron. Soc. Australia, 34, e039
Cannon J. M., et al., 2005, ApJ, 630, L37
Cantiello M., et al., 2018, A&A, 611, A93
Carlson M. N., Holtzman J. A., 2001, PASP, 113, 1522
Carretta E., Bragaglia A., Gratton R., Lucatello S., 2009, A&A, 505, 139
Castellanos E., Escamilla-Rivera C., Mastache J., 2020, International Journal of Modern Physics D, 29, 2050063
Chandar R., Tsvetanov Z., Ford H. C., 2001, AJ, 122, 1342
Chandar R., Whitmore B., Lee M. G., 2004, ApJ, 611, 220
Chen Y., Gnedin O. Y., 2022, MNRAS, 514, 4736
Chen Y., Gnedin O. Y., 2023, MNRAS, 522, 5638
Chiboucas K., Karachentsev I. D., Tully R. B., 2009, AJ, 137, 3009
Chies-Santos A. L., Larsen S. S., Cantiello M., Strader J., Kuntschner H., Wehner E. M., Brodie J. P., 2012, A&A, 539, A54
Choksi N., Gnedin O. Y., 2019, MNRAS, 488, 5409
Choksi N., Gnedin O. Y., Li H., 2018, MNRAS, 480, 2343
Cole D. R., Dehnen W., Read J. I., Wilkinson M. I., 2012, MNRAS, 426, 601
Coles J. P., Read J. I., Saha P., 2014, MNRAS, 445, 2181
Comparat J., Prada F., Yepes G., Klypin A., 2017, MNRAS, 469, 4157
Cook D. O., et al., 2014, MNRAS, 445, 881
Côté P., 1999, AJ, 118, 406
Courteau S., et al., 2014, Reviews of Modern Physics, 86, 47
Crnojević D., Sand D. J., Zaritsky D., Spekkens K., Willman B., Hargis J. R., 2016, ApJ, 824, L14
D'Antona F., Caloi V., 2007, Proceedings of the International Astronomical Union, 3, 156
Da Costa G. S., Grebel E. K., Jerjen H., Rejkuba M., Sharina M. E., 2009, AJ, 137, 4361
Dalcanton J. J., et al., 2009, ApJS, 183, 67
Deason A., Wetzel A., Garrison-Kimmel S., 2014, ApJ, 794, 115
Deason A. J., Wetzel A. R., Garrison-Kimmel S., Belokurov V., 2015, MNRAS, 453, 3568
Diemer B., Joyce M., 2019, ApJ, 871, 168
Doppel J. E., Sales L. V., Navarro J. F., Abadi M. G., Peng E. W., Toloba E., Ramos-Almendares F., 2021, MNRAS, 502, 1661

Dornan V., Harris W. E., 2023, ApJ, 950, 179

Dutton A. A., Macciò A. V., 2014, Monthly Notices of the Royal Astronomical Society, 441, 3359

Eadie G. M., Harris W. E., Springford A., 2022, ApJ, 926, 162

El-Badry K., Quataert E., Weisz D. R., Choksi N., Boylan-Kolchin M., 2019, MNRAS, 482, 4528

Evans A. J., Strigari L. E., Zivick P., 2022, MNRAS, 511, 4251

Fahrion K., et al., 2020, A&A, 637, A27

Fall S. M., Zhang Q., 2001, ApJ, 561, 751

Fleming S. W., et al., 2015, in American Astronomical Society Meeting Abstracts #225. p. 336.59

Forbes D. A., 2005, ApJ, 635, L137

Forbes D. A., Bridges T., 2010, MNRAS, 404, 1203

Forbes D. A., Remus R.-S., 2018, MNRAS, 479, 4760

Forbes D. A., Brodie J. P., Huchra J., 1997, AJ, 113, 887

Forbes D. A., et al., 2018a, Proceedings of the Royal Society of London Series A, 474, 20170616

Forbes D. A., Read J. I., Gieles M., Collins M. L. M., 2018b, Monthly Notices of the Royal Astronomical Society, 481, 5592

Forbes D. A., Alabi A., Romanowsky A. J., Brodie J. P., Arimoto N., 2020, MNRAS, 492, 4874

Foreman-Mackey D., Hogg D. W., Lang D., Goodman J., 2013, PASP, 125, 306

Galleti S., Federici L., Bellazzini M., Buzzoni A., Pecci F. F., 2006, The Astrophysical Journal, 650, L107

Gebhardt K., Kissler-Patig M., 1999, AJ, 118, 1526

Georgiev T. B., Tikhonov N. A., Karachentsev I. D., Ivanov V. D., 1996, Astronomical and Astrophysical Transactions, 11, 39

Georgiev I. Y., Puzia T. H., Hilker M., Goudfrooij P., 2009, MNRAS, 392, 879

Georgiev I. Y., Puzia T. H., Goudfrooij P., Hilker M., 2010, MNRAS, 406, 1967

Girelli G., Pozzetti L., Bolzonella M., Giocoli C., Marulli F., Baldi M., 2020, A&A, 634, A135

González-Lópezlira R. A., et al., 2017, ApJ, 835, 184

Goudfrooij P., Strader J., Brenneman L., Kissler-Patig M., Minniti D., Huizinga J. E., 2003, Monthly Notices of the Royal Astronomical Society, 343, 665

Gratton R., Sneden C., Carretta E., 2004, ARA&A, 42, 385

Harris W. E., 1991, ARA&A, 29, 543

Harris W. E., 1996, AJ, 112, 1487

Harris W. E., 2010, arXiv e-prints, p. arXiv:1012.3224

Harris W. E., 2023, ApJS, 265, 9

Harris W. E., Pudritz R. E., 1994, ApJ, 429, 177

Harris W. E., van den Bergh S., 1981, AJ, 86, 1627

Harris W. E., Harris G. L. H., Alessi M., 2013, ApJ, 772, 82

Harris W. E., et al., 2014, ApJ, 797, 128

Harris W. E., Harris G. L., Hudson M. J., 2015, ApJ, 806, 36

Harris W. E., Blakeslee J. P., Harris G. L. H., 2017, ApJ, 836, 67

Harris C. R., et al., 2020, Nature, 585, 357

Hartman K., Harris W. E., Blakeslee J. P., Ma C.-P., Greene J. E., 2023, ApJ, 953, 154

Hazra N., Cantiello M., Raimondo G., Mirabile M., Blakeslee J. P., Branchesi M., Brocato E., 2022, A&A, 666, A99

Hilker M., Richtler T., 2000, A&A, 362, 895

Ho L. C., Filippenko A. V., 1996, ApJ, 466, L83

Hodge P. W., Dolphin A. E., Smith T. R., Mateo M., 1999, ApJ, 521, 577

Holwerda B. W., 2005, Source Extractor for Dummies v5, doi:10.48550/ARXIV.ASTRO-PH/0512139, https://arxiv.org/abs/astro-ph/0512139

Hudson M. J., Harris G. L., Harris W. E., 2014, ApJ, 787, L5

Hunter J. D., 2007, Computing in Science & Engineering, 9, 90

Huxor A. P., Tanvir N. R., Irwin M. J., Ibata R., Collett J. L., Ferguson A. M. N., Bridges T., Lewis G. F., 2005, MNRAS, 360, 1007

Hwang N., Lee M. G., 2006, ApJ, 638, L79

Hwang N., Lee M. G., Lee J. C., Park W.-K., Park H. S., Kim S. C., Park J.-H., 2011, ApJ, 738, 58

Ivans I. I., Sneden C., Kraft R. P., Suntzeff N. B., Smith V. V., Langer G. E., Fulbright J. P., 1999, AJ, 118, 1273

Jordán A., et al., 2007, ApJS, 171, 101

Joye W. A., Mandel E., 2003, in Payne H. E., Jedrzejewski R. I., Hook R. N., eds, Astronomical Society of the Pacific Conference Series Vol. 295, Astronomical Data Analysis Software and Systems XII. p. 489

Kissler-Patig M., 2000, Reviews in Modern Astronomy, 13, 13

Kissler-Patig M., Brodie J. P., Schroder L. L., Forbes D. A., Grillmair C. J., Huchra J. P., 1998, AJ, 115, 105

Kruijssen J. M. D., 2014, Classical and Quantum Gravity, 31, 244006

Kruijssen J. M. D., Pelupessy F. I., Lamers H. J. G. L. M., Portegies Zwart S. F., Bastian N., Icke V., 2012, MNRAS, 421, 1927

Kundu A., Whitmore B. C., 2001, AJ, 121, 2950

Larsen S. S., Brodie J. P., Huchra J. P., Forbes D. A., Grillmair C. J., 2001, AJ, 121, 2974

Larsen S. S., Brodie J. P., Hunter D. A., 2004, AJ, 128, 2295

Leaman R., 2012, AJ, 144, 183

Lee H., Skillman E. D., Cannon J. M., Jackson D. C., Gehrz R. D., Polomski E. F., Woodward C. E., 2006, The Astrophysical Journal, 647, 970

Li H., Gnedin O. Y., 2014, ApJ, 796, 10

Lim S., Peng E. W., Côté P., Sales L. V., den Brok M., Blakeslee J. P., Guhathakurta P., 2018, ApJ, 862, 82

Lomelí-Núñez L., Mayya Y. D., Rodríguez-Merino L. H., Ovando P. A., Rosa-González D., 2022, MNRAS, 509, 180

Ma J., Zhou X., Chen J., Wu Z., Yang Y., Jiang Z., Wu J., 2005, Publications of the Astronomical Society of the Pacific, 117, 256

Mackey A. D., van den Bergh S., 2005, MNRAS, 360, 631

Mackey A. D., et al., 2013, ApJ, 770, L17

Majewski S. R., Patterson R. J., Dinescu D. I., Johnson W. Y., Ostheimer J. C., Kunkel W. E., Palma C., 2000, in Noels A., Magain P., Caro D., Jehin E., Parmentier G., Thoul A. A., eds, Liege International Astrophysical Colloquia Vol. 35, Liege International Astrophysical Colloquia. p. 619 (arXiv:astro-ph/9910278), doi:10.48550/arXiv.astro-ph/9910278

Marino A. F., et al., 2012, ApJ, 746, 14

Martin N. F., et al., 2016, ApJ, 833, 167

Martínez-Delgado D., et al., 2012, ApJ, 748, L24

McLaughlin D. E., van der Marel R. P., 2005, ApJS, 161, 304

Mészáros S., et al., 2015, AJ, 149, 153

Meurer G. R., Heckman T. M., Leitherer C., Kinney A., Robert C., Garnett D. R., 1995, AJ, 110, 2665

Miller B. W., Lotz J. M., 2007, ApJ, 670, 1074

Mondal C., Subramaniam A., George K., 2021, Journal of Astrophysics and Astronomy, 42, 50

Mucciarelli A., Massari D., Minelli A., Romano D., Bellazzini M., Ferraro F. R., Matteucci F., Origlia L., 2021, Nature Astronomy, 5, 1247

Muratov A. L., Gnedin O. Y., 2010, ApJ, 718, 1266

Nantais J. B., Huchra J. P., McLeod B., Strader J., Brodie J. P., 2010, AJ, 139, 1413

Nantais J. B., Huchra J. P., Zezas A., Gazeas K., Strader J., 2011, AJ, 142, 183

Nataf D. M., et al., 2019, AJ, 158, 14

Navarro J. F., Frenk C. S., White S. D. M., 1996, ApJ, 462, 563

Oh S.-H., Brook C., Governato F., Brinks E., Mayer L., de Blok W. J. G., Brooks A., Walter F., 2011, AJ, 142, 24

Orkney M. D. A., Read J. I., Petts J. A., Gieles M., 2019, MNRAS, 488, 2977

Osborn T. W., Schmitt R. A., 1971, Meteoritics, 6, 297

Pan J., et al., 2022, MNRAS, 515, 48

Pasquali A., et al., 2008, ApJ, 687, 1004

Peñarrubia J., Walker M. G., Gilmore G., 2009, MNRAS, 399, 1275

Peacock M. B., Maccarone T. J., Knigge C., Kundu A., Waters C. Z., Zepf S. E., Zurek D. R., 2010, MNRAS, 402, 803

Pellerin A., Meyer M. M., Calzetti D., Harris J., 2012, AJ, 144, 182

Peng E. W., et al., 2006, ApJ, 639, 95

Peng E. W., et al., 2008, ApJ, 681, 197

Perrett K. M., Bridges T. J., Hanes D. A., Irwin M. J., Brodie J. P., Carter D., Huchra J. P., Watson F. G., 2002, AJ, 123, 2490

Piotto G., et al., 2007, ApJ, 661, L53

Portegies Zwart S. F., McMillan S. L. W., Gieles M., 2010, ARA&A, 48, 431

Prole D. J., et al., 2019, MNRAS, 484, 4865

Puzia T. H., Kissler-Patig M., Thomas D., Maraston C., Saglia R. P., Bender R., Goudfrooij P., Hempel M., 2005, A&A, 439, 997

Read J. I., Iorio G., Agertz O., Fraternali F., 2017, MNRAS, 467, 2019

Reed L. G., Harris G. L. H., Harris W. E., 1994, AJ, 107, 555

Reina-Campos M., Keller B. W., Kruijssen J. M. D., Gensior J., Trujillo-Gomez S., Jefferson S. M. R., Pfeffer J. L., Sills A., 2022, MNRAS, 517, 3144

Rich R. M., Collins M. L. M., Black C. M., Longstaff F. A., Koch A., Benson A., Reitzel D. B., 2012, Nature, 482, 192

Richtler T., 2003, in , Stellar Candles for the Extragalactic Distance Scale. Springer Berlin Heidelberg, pp 281–305, doi:10.1007/978-3-540-39882-0_15, https://doi.org/10.1007%2F978-3-540-39882-0_15

Santiago B. X., Djorgovski S., 1993, Monthly Notices of the Royal Astronomical Society, 261, 753

Santiago-Corté s M., Mayya Y. D., Rosa-González D., 2010, Monthly Notices of the Royal Astronomical Society

Schlegel D. J., Finkbeiner D. P., Davis M., 1998, ApJ, 500, 525

Secker J., 1992, AJ, 104, 1472

Sharina M. E., Puzia T. H., Makarov D. I., 2005, A&A, 442, 85

Shetrone M. D., 1996, AJ, 112, 2639

Sigad Y., Kolatt T. S., Bullock J. S., Kravtsov A. V., Klypin A. A., Primack J. R., Dekel A., 2000, Velocity and Mass Functions of Galactic Halos: Evolution and Environmental Dependence, doi:10.48550/ARXIV.ASTRO-PH/0005323, https://arxiv.org/abs/astro-ph/0005323

Simanton L. A., Chandar R., Whitmore B. C., 2015, ApJ, 805, 160

Sirianni M., et al., 2005, Publications of the Astronomical Society of the Pacific, 117, 1049

Skillman E., 2005, Quantifying Star Formation and Feedback: The M81 Group Dwarf Galaxies, HST Proposal ID 10605. Cycle 14

Smithsonian Astrophysical Observatory 2000, SAOImage DS9: A utility for displaying astronomical images in the X11 window environment, Astrophysics Source Code Library, record ascl:0003.002 (ascl:0003.002)

Sorgho A., Foster T., Carignan C., Chemin L., 2019, MNRAS, 486, 504

Sorgho A., Chemin L., Kam Z. S., Foster T., Carignan C., 2020, MNRAS, 493, 2618

Spitler L. R., Forbes D. A., 2009, Monthly Notices of the Royal Astronomical Society: Letters, 392, L1

Strader J., Brodie J. P., Cenarro A. J., Beasley M. A., Forbes D. A., 2005, AJ, 130, 1315

Trujillo-Gomez S., Kruijssen J. M. D., Keller B. W., Reina-Campos M., 2021, MNRAS, 506, 4841

Tudorica A., Georgiev I. Y., Chies-Santos A. L., 2015, A&A, 581, A84

Veljanoski J., et al., 2015, MNRAS, 452, 320

Villegas D., Kissler-Patig M., Jordán A., Goudfrooij P., Zwaan M., 2008, AJ, 135, 467

Villegas D., et al., 2010, ApJ, 717, 603

Virtanen P., et al., 2020, Nature Methods, 17, 261

Walter F., 2003, Investigating the Powering Sources of Expanding Supergiant Shells in the Nearby Dwarf Galaxy IC 2574, HST Proposal ID 9755. Cycle 12

Watson A. M., et al., 1996, AJ, 112, 534

Wechsler R. H., Tinker J. L., 2018, ARA&A, 56, 435

Weinmann S. M., Franx M., van Dokkum P., Bezanson R., 2013, ApJ, 767, L21

Weisz D. R., Skillman E. D., Cannon J. M., Dolphin A. E., Kennicutt Robert C. J., Lee J., Walter F., 2008, ApJ, 689, 160

Wenger M., et al., 2000, A&AS, 143, 9

Wes McKinney 2010, in Stéfan van der Walt Jarrod Millman eds, Proceedings of the 9th Python in Science Conference. pp 56 – 61, doi:10.25080/Majora-92bf1922-00a

West M. J., Jordán A., Blakeslee J. P., Côté P., Gregg M. D., Takamiya M., Marzke R. O., 2011, A&A, 528, A115

Wetzel A. R., Deason A. J., Garrison-Kimmel S., 2015, ApJ, 807, 49

Wheeler C., Oñorbe J., Bullock J. S., Boylan-Kolchin M., Elbert O. D., Garrison-Kimmel S., Hopkins P. F., Kereš D., 2015, MNRAS, 453, 1305

Whitmore B. C., Sparks W. B., Lucas R. A., Macchetto F. D., Biretta J. A., 1995, ApJ, 454, L73

Yong D., Grundahl F., Lambert D. L., Nissen P. E., Shetrone M. D., 2003, A&A, 402, 985

Youakim K., Lind K., Kushniruk I., 2023, MNRAS, 524, 2630

Zepf S. E., Ashman K. M., 1993, MNRAS, 264, 611

de Grijs R., Anders P., Zackrisson E., Östlin G., 2013, MNRAS, 431, 2917

van Dokkum P., et al., 2018a, Nature, 555, 629

van Dokkum P., et al., 2018b, ApJ, 856, L30

van Dokkum P., Danieli S., Abraham R., Conroy C., Romanowsky A. J., 2019a, ApJ, 874, L5

van Dokkum P., et al., 2019b, ApJ, 880, 91

van den Bergh S., 2001, ApJ, 559, L113

van den Bergh S., Mackey A. D., 2004, MNRAS, 354, 713

This paper has been typeset from a TEX/LATEX file prepared by the author.